Progress In Electromagnetics Research C, Vol. 39, 209–224, 2013

A COPLANAR WAVEGUIDE FED ULTRA WIDEBAND HEXAGONAL SLOT ANTENNA WITH DUAL BAND REJECTION

Tapan Mandal[1, *] and Santanu Das[2]

[1]Department of Information Technology, Government College of Engineering and Textile Technology, Serampore, Hooghly, PIN-712201, India

[2]Department of Electronics & Tele-Comm. Engineering, Bengal Engineering and Science University, Shibpur, Howrah, PIN-711103, India

Abstract—In this paper a printed regular hexagonal slot antenna with a hexagonal stub fed by a coplanar waveguide line has been considered for ultra wide bandwidth. This antenna is then modified to obtain dual band rejection. The Wireless Local Area Network (WLAN) and Wireless Microwave Access (WiMAX) band rejections are realized by incorporating a C-shape slot within the exciting stub as well as a couple of Z-shape open circuit stubs symmetrically inserted at the edge of the slot. The length and width of the C-shape slot and Z-shape stub offer sufficient freedom for selecting and shifting the notch bands. Magnitude of S_{11}, impedance, gain and radiation characteristics of them are studied and discussed here. From the measured results, it has been observed that the impedance bandwidth, defined by magnitude of $S_{11} \leqslant -10\,\text{dB}$, reaches a value of 8.18 GHz (2.96 $\sim$ 11.14 GHz) except dual frequency stop bands of 3.28–3.7 GHz and 5.1–5.90 GHz. From the experimental results, it is observed that the radiation patterns are omnidirectional in the H-plane and dipole in nature in the E-plane. The antenna gain varies from 4.8 dB to 5.3 dB over the whole operating band excluding the notch bands. Surface current distributions are used to analyze the effects of the C-slot and Z-shape stub. Measured group delay has very small variation within the operating band except notch bands and hence the proposed antenna may be suitable for UWB applications.

Received 7 March 2013, Accepted 26 April 2013, Scheduled 5 May 2013

* Corresponding author: Tapan Mandal (tapanmandal20@rediffmail.com).

1. INTRODUCTION

Communication in the Ultra-Wide Band (UWB) range is very promising in the area of wireless communication technology since the allocation of 3.1–10.6 GHz bandwidth (BW) by the US — Federal Communication Commission [1]. At present many attractive characteristics of UWB technology like low cost, low complexity, low spectral power density, very low interference and extremely high data transmission rates have made it a potential candidate in various wireless communications. Stable radiation patterns, gain flatness, linear phase and small group delay variation are also required to fulfill the requirements for UWB application. This type of antenna has been realized by using either microstrip line [2–7] or coplanar waveguide (CPW) feeding structure [8–15]. Microstrip fed rectangular [2, 3], hexagonal [4], ellipse [5, 6], circular [6, 7] wide slot antennas are found to have 10 dB return loss BW for UWB application. However, CPW fed printed slot (aperture) antennas with different structures and performances have been developed [8–15]. In particular researchers and industry people pay much attention in CPW fed antennas because of their several attractive features such as, simple structure with single metallic layer, low radiation loss and easy integration with integrated circuits [8–10]. Besides the cost of the antenna being very low, it can be easily fabricated by using the PCB technology. The UWB antenna has numerous applications such as remote sensing, radar, imaging, localization and medical applications.

In this paper a printed hexagonal slot (aperture) antenna with a hexagonal stub is proposed for UWB applications. The patch (stub) is fed by a CPW line such that only a single-layer metallization substrate is required for this antenna.

However, the existing Wireless Local Area Network (WLAN: IEEE 802.11a) and Wireless Microwave Access (WiMAX: IEEE 802.16) service bands of 5.15–5.88 GHz and 3.3–3.7 GHz are responsible for the performance degradation of UWB system because of the interference. To overcome this problem, an UWB with band rejection characteristics is desirable. The band notch performance is achieved by introducing slots or slits on the radiator [5], placing parasitic strips in close proximity to the antenna [11, 14]. To design slot antennas with band notch function, one simple and effective way is to incorporate slots (known as half-wave resonant structures) in the antenna's tuning stub with U-shape [15], T-shape [8], C-shape slots [8, 12] etc.. In this paper UWB antenna with dual notch band has been proposed by using the above technique. The band stop response (WLAN stop band) is achieved by etching a thin C-slot on the exciting stub. A

pair of thin open Z-shape stub is placed in the slot area to reject the WiMAX band. The slot and stub creates a narrow frequency rejection without disturbing the rest of the operating frequencies and radiation performances. Tuning effects of major parameters on the stop band performance are simulated and also analyzed. Compared to the circular and elliptical slots [6, 7, 13, 15], the proposed hexagonal shape slot with hexagonal stub has two main advantages. These are:

1. The antenna can be simply extended to the advanced band notch design without changing the dimensions of the exciting stub as well as slot of the prototype antenna.
2. The computation time is less for optimization of process.

All of the simulations are carried out using a Method of Moment (MoM) based IE3D^{TM} simulation software [16]. Magnitude of S_{11}, input impedance, gain and radiation pattern, group delay and phase characteristics are studied and analyzed.

2. ANTENNA DESIGN CONSIDERATIONS

2.1. Prototype Antenna Design

For UWB antennas lower band edge frequency and entire bandwidth (BW) become the design parameters instead of resonant or operating frequency [6]. Fig. 1 shows the geometry of prototype antenna which is designed on a substrate having dielectric constant $(\varepsilon_r) = 2.5$, thickness $(h) = 0.79$ mm and loss tangent $(\tan\delta) = 0.002$. The lower frequency (f_l) has been determined using a formula [12] given in Equation (1)

$$R_s \cong \frac{c}{4f_l}\sqrt{\frac{2}{(1+\varepsilon_{reff})}} \tag{1}$$

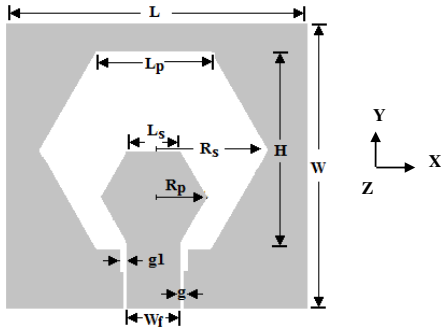

Figure 1. Prototype of regular hexagonal slot antenna.

where $\varepsilon_{reff} = \frac{1+\varepsilon_r}{2}$ is the effective relative permittivity. c and R_s are velocity of light and aperture radius respectively.

Here side length of the aperture (L_p) is related to the aperture radius (R_s) and height of the slot (H) is related to the side length as given follows

$$L_p = R_s \tag{2}$$

$$H = \sqrt{3}L_p \tag{3}$$

where L_p and H are the side length and height of hexagonal slot.

The hexagonal exciting stub dimension is then considered with respect to the aperture radius as

$$R_p = \frac{R_s}{2} \tag{4}$$

The radiating element, namely the slot (aperture) is chosen hexagonal in the investigation in order to achieve a wide BW. A 50 Ω CPW transmission line is designed having a strip width of 3.8 mm. The gap between the feed line and the coplanar ground plane is 0.4 mm. The detailed dimensions are shown in Table 1.

Table 1. Optimized parameter for the proposed antenna.

Parameter	L	W	$R_s = L_p$	$L_s = R_p$	H	T	W_f	g	g_1
Dimension (mm)	42	38	15.25	7	26.4	0.775	7	0.4	0.7
Parameter	L_1	L_2	L_3	L_4	L_5	L_6	W_1	W_2	g_3
Dimension (mm)	7.5	4	1	13	2	1.5	0.3	1	0.5

2.2. Band Notch Design

In another form (Fig. 2) the hexagonal slot antenna is made on the same substrate with the dimensions same as before. In order to reject WLAN band frequencies a thin C-slot is made on the exciting stub. Usually, the length of the slot is made approximately equal to half of the guided wavelength (λ_g) at the notch frequency of the band. This is given by

$$L_{total} = \frac{\lambda_g}{2} = \frac{c}{2f_{notch}\sqrt{\frac{(\varepsilon_r+1)}{2}}} \tag{5}$$

$$L_{total} = 2 \cdot L_1 + 2 \cdot L_2 - L_3 \tag{6}$$

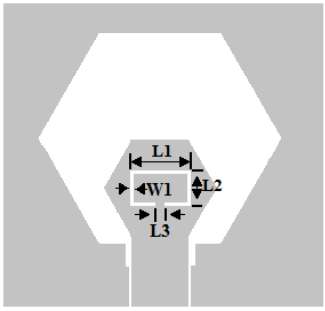

Figure 2. Prototype of hexagonal slot antenna with C-slot.

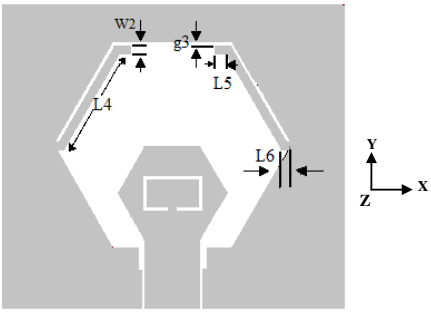

Figure 3. Geometry of proposed antenna with C-slot and Z-shape stub.

where L_{total} is the length of the slot. Corresponding to $f_{notch} = 5.5\,\text{GHz}$, the lengths of the slots can be calculated as 20.6 mm. The optimum slot width is found to be 0.3 mm by way of simulation.

In addition to this WiMAX stop band is realized by symmetrically inserting a pair of narrow open circuited Z-shape stubs on both sides of the aperture area (Fig. 3). Each stub has length of quarter wavelength at desired notch frequency. The center rejected frequencies for the stop band may be empirically approximated by

$$Z_{total\_WiMAX} = \frac{\lambda_g}{4} = \frac{c}{4f_{notch\_WiMAX}\sqrt{\frac{(\varepsilon_r+1)}{2}}} \tag{7}$$

$$Z_{total\_WiMAX} = L4 + L5 + L6 \tag{8}$$

where Z_{total_WiMAX} is the length of the stub. For center notch $f_{notch\_WiMAX} = 3.5\,\text{GHz}$, the length of the stub can be determined as 16.2 mm. The optimum strip width is found to be 1 mm. From Equations (5) to (8), the total length of the C-shape slot and Z-shape stubs may be obtained at the beginning of the design. Finally the lengths are adjusted by using simulator to achieve the desired results.

3. PARAMETRIC STUDY AND DISCUSSION

Figure 1 shows configuration of the prototype antenna. The effects of extrusion depth T on the input impedance are simulated and shown in Fig. 4. It is observed that the T mainly influences the impedance on higher frequencies (6–10.4 GHz). The hexagonal aperture (R_s) is important for the lower frequency. As the slot radius value (R_s)

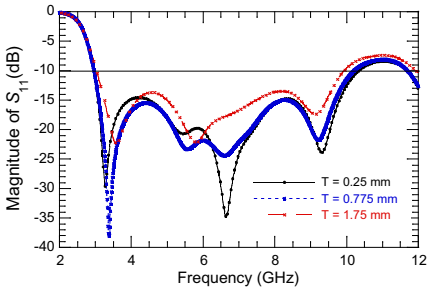

Figure 4. Simulated magnitude of S_{11} for different T.

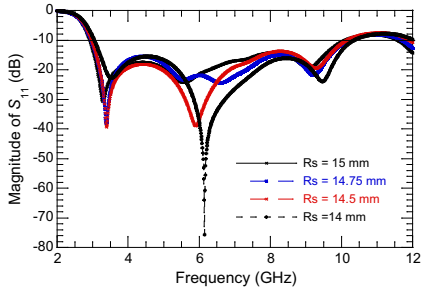

Figure 5. Simulated magnitude of S_{11} for different R_s.

increases, the lower frequency is shifted to the left side of the magnitude of S_{11} plot (Fig. 5). Thus slot radius plays a significant role for selecting the lower edge frequency of the band. The step type ground plane near the feed is considered for impedance matching resulting in wide BW (Fig. 6). Fig. 7 indicates that the hexagonal stub mainly influences the impedance at lower frequencies (3.8–4.6 GHz). From the surface current distribution, it has been observed that the hexagonal slot produces resonance at lower frequency. The hexagonal stub yields second resonance and steps in the ground plane are responsible for the third one.

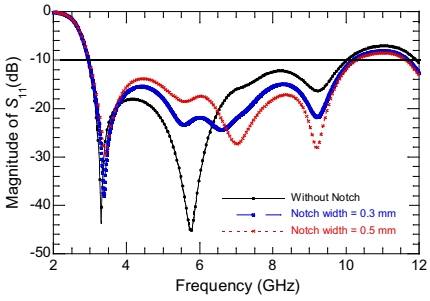

Figure 6. Simulated magnitude of S_{11} for different notch width and without notch.

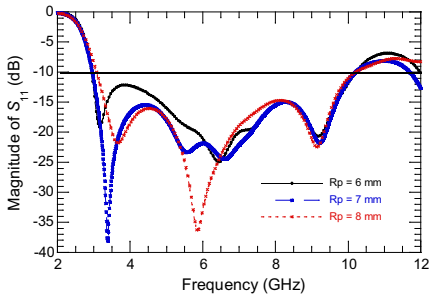

Figure 7. Simulated magnitude of S_{11} for different R_p.

Next the parametric study and discussions are carried out for the antenna with WLAN band rejection (Fig. 2). The C-slot configuration on hexagonal stub has been used independently to obtain WLAN stop band. Here the simulated magnitude of S_{11} characteristics for various values of slot length (L_{total}) and width (W_1) are shown in Figs. 8

and 9 respectively. As the total slot length rises, the stop band region moves toward the lower frequency with higher peak. Slot length has greater impact than slot width (W_1) on shifting the frequency as is evident from Figs. 8 and 9. Due to the presence of C-slot inside the patch, maximum current flows back to the feeding part and degenerates radiation around 5.15 GHz to 5.8 GHz.

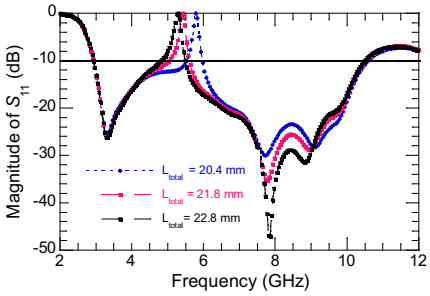

Figure 8. Magnitude of S_{11} for various lengths of L_{total} of C-slot.

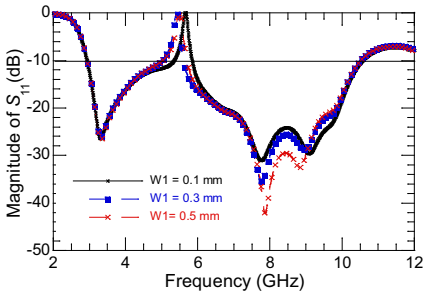

Figure 9. Magnitude of S_{11} for various width of C-slot.

Furthermore to realize the WiMAX stop band in UWB region a pair of Z-shape strips has been used in the slot area. The magnitude of S_{11} plots for various length and width are illustrated in Figs. 10 and 11 respectively. From the simulation result, it has been observed that the length has enough control for shifting and selecting the notch frequency. Magnitude of S_{11} characteristics for all configurations is illustrated in Fig. 12 for comparison. The simulation responses of prototype antenna exhibit 7.6 GHz (3.0 $\sim$ 10.6 GHz) impedance BW for $T = 0.775$ mm, $R_s = 15.25$ mm, $R_p = 7$ mm,

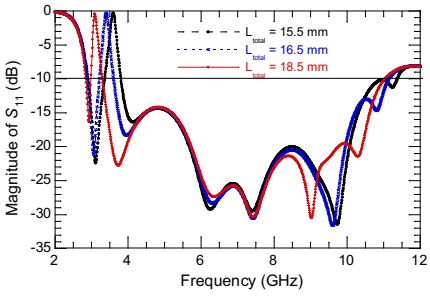

Figure 10. Magnitude of S_{11} for various length of Z-strip.

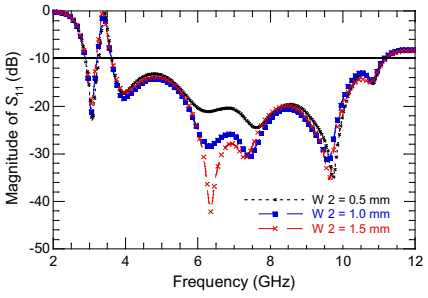

Figure 11. Magnitude of S_{11} for various width of Z-strip.

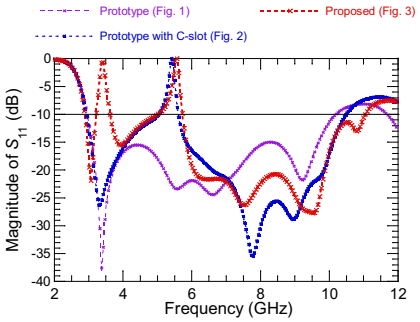

Figure 12. Magnitude of S_{11} characteristics of all configurations for comparisons.

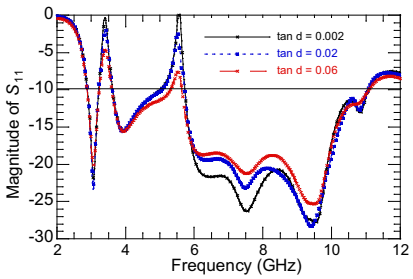

Figure 13. Magnitude of S_{11} versus frequency plot for various values of loss tangent.

$g = 0.4\,\text{mm}$, $g_1 = 0.7\,\text{mm}$ and $W_f = 7\,\text{mm}$. The simulated magnitude of S_{11} characteristics of the proposed antenna reveals stop bands of 0.4 GHz (3.3–3.7 GHz) and 0.65 GHz (5.15-5.8 GHz) for magnitude of $S_{11} \leq -10\,\text{dB}$ within the frequency span from 2.98 GHz to 11.06 GHz. Fig. 13 indicates the simulated magnitude of S_{11} versus frequency characteristics of the proposed antenna for various values of loss tangent. From the characteristics, it is observed that the peak value of S_{11} at notch frequency decreases while the loss tangent of the substrate increases.

4. FABRICATION AND MEASUREMENTS

Photograph of the prototype and proposed antenna are shown in Fig. 14. The following antennas are fabricated on the same specification substrate as mentioned in Section 2. An Agilent make (Model: N5230A) vector network analyzer is used for S_{11} measurement.

The simulated and measured performances of prototype antenna without any slot or strips (Fig. 14(a)) are plotted in Fig. 15 for comparisons. The experimental response yields 8.58 GHz (3.0 GHz–11.58 GHz) impedance band. The simulated result of a prototype antenna without notch characteristics is also shown for comparison. It is clear that the measured result shows a reasonably agreement with simulated one. Thus it may be considered as a good UWB antenna. The discrepancy between simulation and measurement is due to highly sensitive impedance matching requirement which may not be available in the fabricated structure.

The simulated and measured impedance responses of Fig. 14(b) are shown in Fig. 16. The simulated impedance characteristic reveals

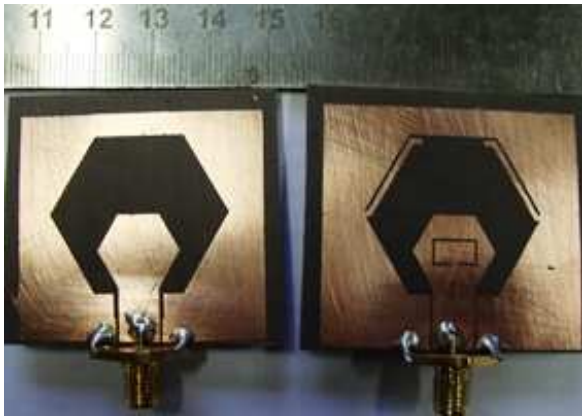

(a) (b)

Figure 14. Fabricated structure of (a) prototype, (b) proposed.

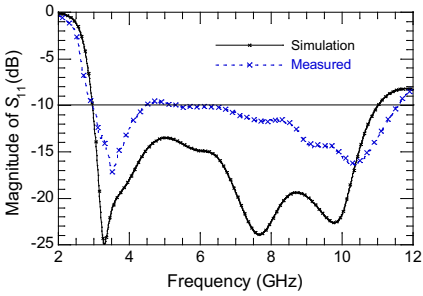

Figure 15. Measured and simulated magnitude of S_{11} of the prototype antenna.

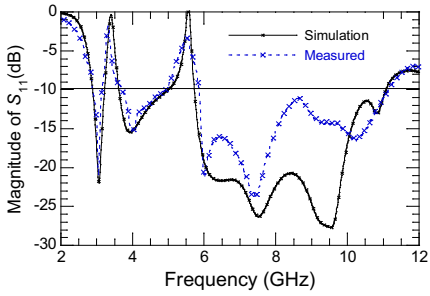

Figure 16. Measured and simulated magnitude of S_{11} of the proposed antenna.

stop bands of 0.40 GHz (3.3–3.70 GHz), 0.65 GHz (5.15–5.8 GHz) for magnitude of $S_{11} \leq -10$ dB within the frequency span from 2.98 GHz to 11.06 GHz while the measured characteristic shows 0.42 GHz (3.28–3.70 GHz) and 0.80 GHz (5.10–5.90 GHz) stop bands which cover the entire WiMAX and WLAN band in the frequency region of 2.96 GHz to 11.14 GHz. The measured result agrees with simulated result which has frequency stop bands of WiMAX and WLAN bands when the C-slot is inserted on the hexagonal patch and two stubs (Z-shape) are placed in the slot area. But 2.5 dB higher S_{11} peak value is obtained at 5.5 GHz in simulation ignoring other associated effects in practical structure. The loss tangent of the substrate and dimensional mismatch

of practical structure may cause the difference between simulated and measured results at the second notch frequency (5.5 GHz).

5. RADIATION PATTERN

The measured radiation patterns at 3.1 GHz and 8.5 GHz are shown in Fig. 17 which has been taken out in a real environment. At lower frequencies H-plane radiation patterns are omnidirectional whereas in E-plane, it is figure of eight because of ground plane on the same side of stub. At higher frequencies, radiation patterns are deteriorating because the equivalent radiating area changes with frequency over UWB. Unequal phase distribution and significant magnitude of higher

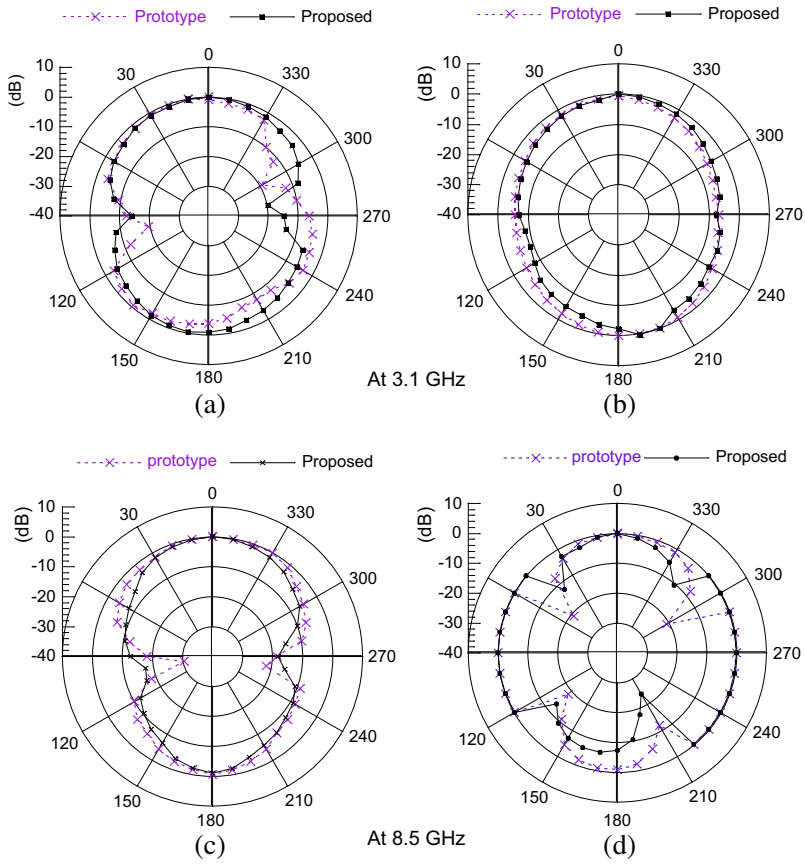

Figure 17. Measured radiation pattern characteristics for prototype (Fig. 14(a)) and proposed antenna (Fig. 14(b)). (a) E-plane pattern, (b) H-plane pattern, (c) E-plane pattern, (d) H-plane pattern.

order modes at higher frequencies also play a part in the deterioration of radiation pattern. In comparison between Figs. 17(b) and 17(d), RF ripple appears in the plot at higher frequency. The RF ripples in the radiation pattern may be due to the reflections into the field among the antenna under test, reference antenna and some other reflecting objects in the surrounding area. It is noted that adding a slot in the exciting stub and strips in the aperture area does not significantly alter the radiation patterns of the antenna. However the E-plane and H-plane patterns change gradually at a small rate over a large bandwidth from 3.1 GHz to 8.5 GHz. Thus this can be considered as a UWB antenna with WiMAX, WLAN notch band characteristics for UWB application.

6. INPUT IMPEDANCE, GAIN AND EFFICIENCY

The real and imaginary part of the input impedance versus frequency of proposed antenna is shown in Fig. 18. The real part of the antenna impedance varies around 50 Ω, while its imaginary part has small values and oscillates around zero. This is mainly because a continuous coupling is obtained between hexagonal patch and ground plane at different positions and hence matching is achieved for different frequencies. The step in the ground plane creates a capacitive load that neutralizes the inductive nature of the patch antenna to produce nearly-pure resistive input impedance. The impedance of the structure changes acutely making large reflection which results in steep rise of magnitude of S_{11} and also sharp decrease of gain and efficiency as shown in Figs. 19 and 20 respectively. The proposed antenna gain varies from 4.8–5.3 dB over the 2.96–11.14 GHz range except in notch band. Fig. 20 indicates that the proposed antenna has appreciable efficiency over the operating frequency region.

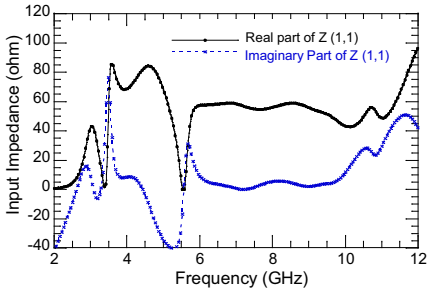

Figure 18. Simulated input impedance of proposed antenna.

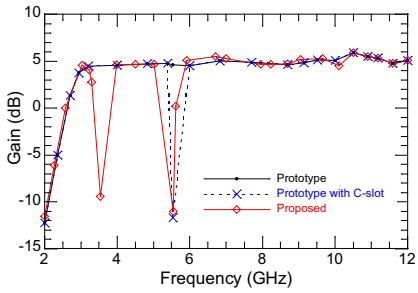

Figure 19. Simulated gain versus frequency plot.

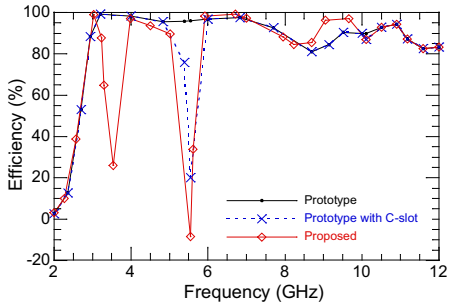

Figure 20. Simulated antenna efficiency versus frequency plot.

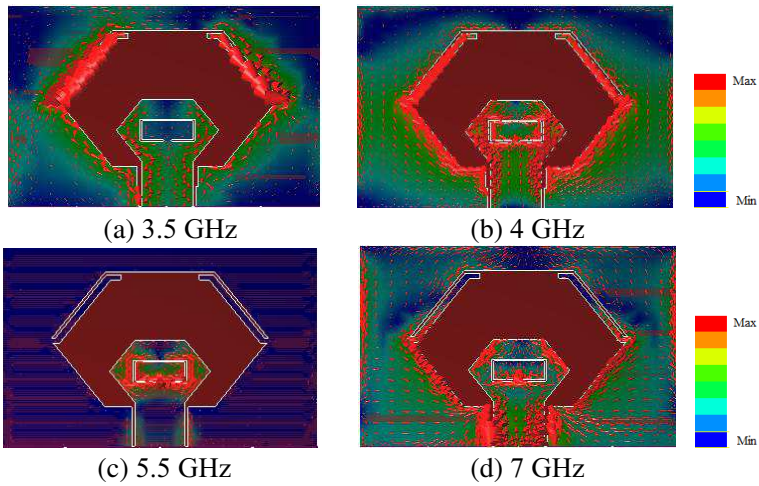

Figure 21. Surface current distributions on the radiating patch at (a) WiMAX notched band at 3.5 GHz, (b) a pass band frequency of 4 GHz, (c) WLAN notched band at 5.5 GHz, (d) a pass band frequency of 7 GHz.

7. CURRENT DISTRIBUTION AND ANALYSIS

Simulated surface current distributions of the proposed antenna at different frequencies are shown in Fig. 21. At a pass band frequency of 4 GHz and 7 GHz (outside the notch band) the distribution of surface current is more or less uniform as is evident in Fig. 21(b) and Fig. 21(d) respectively. At pass band frequencies significant amount of currents are coupling from the exciting stub to ground plane. From Fig. 21(a) and Fig. 21(c), it is observed that the current distribution is

concentrated and oppositely directed on the interior and exterior side of the slot and strips at the notch frequencies. This causes the antenna to operate without significant transmission in the notch band. Therefore slot or strips stops the surface current and as a result notch bands are obtained. At the notch frequency the impedance is nearly infinite impedance (open circuit) at the antenna feeding point. This infinite impedance at the feeding point leads to the impedance mismatching near the notch frequency. Therefore slot and strips behaves as open-circuited series stub with infinite input impedance. So minimum amount of currents are coupling between stub and radiating ground plane. Consequently desired notch bands are created.

8. TRANSFER FUNCTION AND TIME DOMAIN STUDY

Since UWB systems use short pulses to transmit signals, it is crucial to study the transfer function for evaluating the proposed antenna's performance and designing transmitted pulse signals. The group delay is able to show any nonlinearity that may be present in the phase response and indicates the degree of the distortion. For UWB applications, the phase of the transfer function should be linear as much as possible in the operating band. The group delay is required to be constant over the entire band as well.

Agilent make Vector Network Analyzer (N5230A) is used for transfer function measurement and the measurement set up is shown in Fig. 22. A pair of the proposed antenna is used as the transmitting and receiving antenna. The transmitter and receiver are positioned face to face ($+z$ directions opposite) with a distance (D) of 150 mm. By considering the antenna system as a two-port network, the transmission scattering parameter S_{21} which indicates the transfer function is measured. It should be noted that the measurement was carried out in a real environment with reflecting objects in the surrounding area.

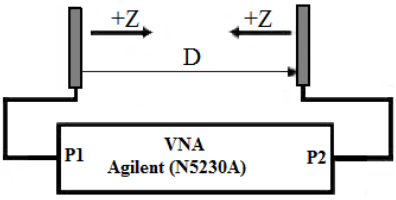

Figure 22. The transfer function measurement set up (Face to face mode).

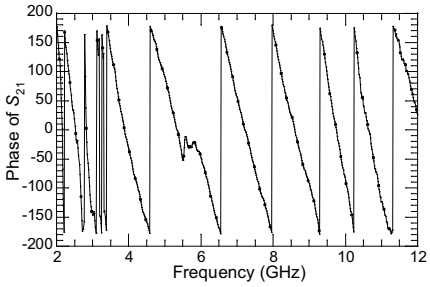

Figure 23. The measured phase of S_{21} for the proposed antenna systems.

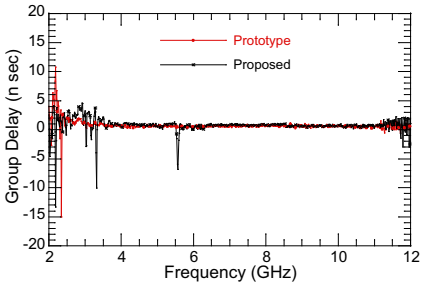

Figure 24. The measured group delay of the antenna systems.

The measured phase of the transfer function is shown in Fig. 23. It is observed that the phase of S_{21} is relatively linear from 2.96 GHz to 11.14 GHz excluding the notch bands in face to face mode. Fig. 24 shows the measured group delay for the antenna system. The variation of group delay for proposed antenna is within 1 ns across the whole UWB band except two notched bands, in which the maximum group delay is more than 10 ns in 3.5 GHz notched band and more than 6 ns in 5.5 GHz notched band. The measured group delay corresponds well to the phase of S_{21}, so it proves that the antenna has a good time-domain characteristic and a small pulse distortion as well.

9. CONCLUSIONS

To mitigate the interferences between the UWB systems and existing WiMAX, WLAN system, a CPW fed slot antenna with dual band rejection has been proposed. Parametric studies of the antenna characteristics are presented. Dual stop bands are realised by etching one C-slot inside exciting stub as well as symmetrically adding a pair of open-circuit stubs at the edge of the slot. Two types of band-notched structures extended from the prototype design are provided and verified. The surface current distributions are used to analyze the physical effect of the slot generating the band notch characteristics. This antenna has ultra wide-band performance in the frequency band of 8.18 GHz (2.96 to 11.14 GHz) for magnitude of $S_{11} \leq -10$ dB with excellent WiMAX and WLAN rejection bands. Variation in the radiation patterns is very small over the UWB region except stop bands. It has been revealed that the antenna has linear phase of transfer function and constant group delay within the operating band except at notched bands which ensures the good linear transmission

performances. Therefore the proposed antenna is expected to be a good candidate in various modern UWB applications.

ACKNOWLEDGMENT

This work was supported by CSIR, New Delhi, India. Sanctioned No. 22(0512)/EMR-II dt. 31.05. 2010.

REFERENCES

1. First Report and Order, "Revision of part 15 of the commission's rule regarding ultra-wideband transmission system FCC 02-48," *Federal Communications Commission*, 2002.
2. Chen, H. D., "Broadband CPW-fed square slot antennas with a widened tuning stub," *IEEE Transaction on Antennas and Propagation*, Vol. 51, No. 8, 1982–1986, 2003.
3. Abdollahv, M., G. Dadashzadeh, and D. Mostafa, "Compact dual band-notched printed monopole antenna for UWB application," *IEEE Antennas and Wireless Propagation Letters*, Vol. 9, 1148–1151, 2010.
4. Ghaderi, M. R. and F. Mohajeri, "A compact hexagonal wide slot antennas with microstrip fed monopole for UWB applications," *IEEE Antenna and Wireless Propagation Letter*, Vol. 10, 682–685, 2011.
5. Liao, X. J., H. C. Yang, N. Han, and Y. Li, "Aperture UWB antenna with triple band-notched characteristics," *Electronics Letters*, Vol. 47, No. 2, 2011.
6. Li, P. C., J. X. Liang, and X. D. Chen, "Study of printed elliptical/circular slot antennas for ultra-wide band applications," *IEEE Transactions on Antennas and Propagation*, Vol. 54, No. 6, 1670–1675, 2006.
7. Barbarino, S. and F. Consoli, "UWB circular slot antenna with an inverted-L notch filter for the 5 GHz WLAN band," *Progress In Electromagnetics Research*, Vol. 104, 1–13, 2010.
8. Cheng, Y. and K.-J. Hung, "Compact ultra-wide band rectangular aperture antenna and band-notched designs," *IEEE Transactions on Antennas and Propagation*, Vol. 54, No. 11, November 2006.
9. Liang, X. L., T. A. Denidni, L. N. Zhang, R. H. Jin, J. P. Geng, and Q. Yu, "Printed binomial curved slot antennas for various wideband applications," *IEEE Transactions on Microwave Theory and Techniques*, Vol. 59, No. 4, 1058–1065, 2011.

10. Chair, R., A. A. Kishk, and K. F. Lee, "Ultra wide band coplanar waveguide-fed rectangular slot antenna," *IEEE Antennas Wireless Propagation Letter*, Vol. 3, No. 12, 227–229, 2004.
11. Moeikham, P., C. Mahatthanajatuphat, and P. Akkaraekthalin, "A compact ultra-wideband monopole antenna with 5.5 GHz notch," *Progress In Electromagnetics Research C*, Vol. 26, 13–27, 2012.
12. Zhu, F., S. Gao, A. T. S. Ho, C. H. See, R. A. Abd Alhameed, J. Li, and J. Xu, "Design and analysis of planar ultra-wideband with dual notched function," *Progress In Electromagnetics Research*, Vol. 127, 523–536, 2012.
13. Habib, M. A., A. Bostani Djaiz, M. Nedil, M. C. E. Yagoub, and T. A. Denidni, "Ultra wideband CPW-fed aperture antenna with WLAN band rejection," *Progress In Electromagnetics Research*, Vol. 106, 17–31, 2010.
14. Islam, M. T., R. Azim, and A. T. Mobashsher, "Triple band-notched planar UWB antenna using parasitic strips," *Progress In Electromagnetics Research*, Vol. 129, 161–179, 2012.
15. Panda, J. R. and R. S. Kshetrimayum, "A compact CPW-fed hexagonal 5 GHz/6 GHz band-notched antenna with an U-shaped slot for ultra-wide band communication systems," *2010 International Conference on Signal Processing and Communications (SPCOM)*, 1–5, 2010 (IEEE 978-1-4244-7138-6/10).
16. Zeland IE3D^{TM} Software.